The Plant Cell, Vol. 25: 2302–2314, June 2013, www.plantcell.org

Structure of the *Arabidopsis* Glucan Phosphatase LIKE SEX FOUR2 Reveals a Unique Mechanism for Starch Dephosphorylation[W]

David A. Meekins,[a,1] Hou-Fu Guo,[a,1] Satrio Husodo,[a] Bradley C. Paasch,[a] Travis M. Bridges,[a] Diana Santelia,[b] Oliver Kötting,[c] Craig W. Vander Kooi,[a,2] and Matthew S. Gentry[a,2,3]

[a] Department of Molecular and Cellular Biochemistry and Center for Structural Biology, University of Kentucky, Lexington, Kentucky 40535-0509

[b] Institute of Plant Biology, University of Zürich, 8092 Zurich, Switzerland.

[c] Institute for Agricultural Sciences, ETH Zürich, 8092 Zurich, Switzerland

Starch is a water-insoluble, Glc-based biopolymer that is used for energy storage and is synthesized and degraded in a diurnal manner in plant leaves. Reversible phosphorylation is the only known natural starch modification and is required for starch degradation in planta. Critical to starch energy release is the activity of glucan phosphatases; however, the structural basis of dephosphorylation by glucan phosphatases is unknown. Here, we describe the structure of the *Arabidopsis thaliana* starch glucan phosphatase LIKE SEX FOUR2 (LSF2) both with and without phospho-glucan product bound at 2.3Å and 1.65Å, respectively. LSF2 binds maltohexaose-phosphate using an aromatic channel within an extended phosphatase active site and positions maltohexaose in a C3-specific orientation, which we show is critical for the specific glucan phosphatase activity of LSF2 toward native *Arabidopsis* starch. However, unlike other starch binding enzymes, LSF2 does not possess a carbohydrate binding module domain. Instead we identify two additional glucan binding sites located within the core LSF2 phosphatase domain. This structure is the first of a glucan-bound glucan phosphatase and provides new insights into the molecular basis of this agriculturally and industrially relevant enzyme family as well as the unique mechanism of LSF2 catalysis, substrate specificity, and interaction with starch granules.

INTRODUCTION

As the major energy cache for plants and algae, starch is a central component of human and animal diets and a key constituent in many manufacturing processes. Starch is composed of two Glc polymers: amylopectin (75 to 90%) and amylose (10 to 25%) (Tester et al., 2004; Streb and Zeeman, 2012). Structurally, amylose is a linear molecule composed of α-1,4-glycosidic–linked chains with few branches, while amylopectin is formed from α-1,4-glycosidic–linked chains with α-1,6-glycosidic branches, similar to glycogen in animal tissues. However, compared with glycogen, the glucan chains composing amylopectin are longer with fewer branches that are organized into clusters at regular intervals (Gallant et al., 1997; Buléon et al., 1998; Roach, 2002). The biophysical properties of amylopectin result in the formation of double helices by adjacent glucan chains that interact to form crystalline lamellae, significantly contributing to the water insolubility of starch (Buléon et al., 1998; Streb and Zeeman, 2012).

Starch is synthesized and degraded in a diurnal manner in plant leaves via the concerted activity of starch synthases, branching enzymes, isoamylases, and amylases (Keeling and Myers, 2010; Streb and Zeeman, 2012). Water insolubility is an essential feature of starch that underlies the ability of starch granules to function in energy storage by regulating the access of starch hydrolyzing enzymes (e.g., amylases) (Caspar et al., 1991; Yu et al., 2001; Blennow and Engelsen, 2010). Reversible starch phosphorylation, via glucan dikinases and phosphatases, is necessary to solubilize glucans in the outer layer of the starch granule and permit their catabolism during nonphotosynthetic periods (Fettke et al., 2009; Blennow and Engelsen, 2010; Kötting et al., 2010; Streb and Zeeman, 2012). Thus, starch degradation is based on a cyclical enzymatic process involving glucan dikinases, amylases, and glucan phosphatases.

In plants, there are two glucan dikinases that phosphorylate starch. α-Glucan water dikinase (GWD) phosphorylates the C6-position of Glc moieties on the starch granule surface, and this event triggers C3-phosphorylation by phosphoglucan water dikinase (PWD) (Ritte et al., 2002; Baunsgaard et al., 2005; Kötting et al., 2005; Ritte et al., 2006). Biophysical studies suggest that C3-phosphorylation imposes steric effects that result in amylopectin helix unwinding and local solubilization of surface glucans, thus permitting amylolytic degradation by β-amylases (Edner et al., 2007; Hansen et al., 2009; Blennow and Engelsen, 2010). However, β-amylase activity is inhibited when a phosphate group is reached; therefore, glucan phosphatases must release phosphate from starch to allow processive starch breakdown (Takeda, 1981; Kötting et al., 2009). Plants contain two glucan phosphatases that dephosphorylate starch and allow further degradation by β-amylase (Niittylä et al., 2006; Gentry et al., 2007; Kötting et al., 2009; Santelia et al., 2011).

[1] These authors contributed equally to this work.
[2] These authors contributed equally to this work.
[3] Address correspondence to matthew.gentry@uky.edu.
The authors responsible for distribution of materials integral to the findings presented in this article in accordance with the policy described in the Instructions for Authors (www.plantcell.org) are Matthew S. Gentry (matthew.gentry@uky.edu) and Craig W. Vander Kooi (craig.vanderkooi@uky.edu).
[W] Online version contains Web-only data.
www.plantcell.org/cgi/doi/10.1105/tpc.113.112706

Glucan phosphatases are members of the protein tyrosine phosphatase (PTP) superfamily characterized by a conserved Cx_5R catalytic motif (Yuvaniyama et al., 1996; Gentry et al., 2007; Tonks, 2013). The PTPs include a heterogeneous group of phosphatases called the dual specificity phosphatases (DSPs) that dephosphorylate phospho-Ser, -Thr, and -Tyr of proteinaceous substrates as well as more diverse substrates such as lipids, nucleic acids, and glucans (Alonso et al., 2003; Tonks, 2006; Moorhead et al., 2009). The glucan phosphatase STARCH EXCESS4 (SEX4) has been shown to preferentially dephosphorylate the C6-position, and LIKE SEX FOUR2 (LSF2) specifically dephosphorylates the C3-position of Glc moieties (Hejazi et al., 2010; Santelia et al., 2011). However, the structural basis for specific glucan phosphatase activity and position specificity has not been determined. LSF2 and SEX4 are DSPs that are conserved in Archaeplastida/Plantae genomes from land plants to single-cell green algae (Gentry et al., 2007; Gentry and Pace, 2009; Santelia et al., 2011). *Arabidopsis thaliana* lacking SEX4 activity have larger starch granules, more leaf starch, and altered patterns of starch phosphorylation, a phenotype further exacerbated upon the simultaneous loss of LSF2 activity (Zeeman et al., 2002; Niittylä et al., 2006; Kötting et al., 2009; Santelia et al., 2011). Furthermore, LSF2 and SEX4 are functionally related to the glycogen phosphatase laforin that is found in all vertebrates and a subset of unicellular protozoa (Worby et al., 2006; Gentry et al., 2007, 2009; Tagliabracci et al., 2007). Mutations in the gene that encodes laforin in humans cause the accumulation of insoluble carbohydrates leading to the fatal epileptic disorder Lafora's disease (Minassian et al., 1998; Serratosa et al., 1999; Gentry et al., 2009). These findings demonstrate that glucan phosphatase activity is highly conserved in nature and essential for both starch and glycogen metabolism.

SEX4 and LSF2 proteins both contain a chloroplast targeting peptide, a DSP domain, and a unique C-terminal (CT) motif (Kerk et al., 2006; Niittylä et al., 2006; Sokolov et al., 2006; Gentry et al., 2007; Kötting et al., 2009; Vander Kooi et al., 2010; Santelia et al., 2011). Chloroplast targeting peptides localize proteins to the chloroplast, the site of starch metabolism. The CT motif was originally identified in the SEX4 structure as a motif that folds into the DSP core and is essential for protein stability and function (Vander Kooi et al., 2010). Additionally, SEX4 contains a carbohydrate binding module (CBM) that is common in starch-interacting enzymes (Niittylä et al., 2006; Sokolov et al., 2006; Gentry et al., 2007; Glaring et al., 2011). CBMs are nonenzymatic domains that typically bind a specific carbohydrate and allow the catalytic portion of the enzyme to modify the substrate (Coutinho and Henrissat, 1999; Boraston et al., 2004; Machovic and Janecek, 2006). The previously determined glucan-free SEX4 structure demonstrated that its CBM and DSP domains interact to form a continuous binding pocket that coordinates the dual functions of glucan binding and dephosphorylation (Vander Kooi et al., 2010). An additional plant protein called LSF1 also contains a CBM and DSP domain (Comparot-Moss et al., 2010). While LSF1 is required for starch degradation, it lacks phosphatase activity and is not considered a glucan phosphatase (Comparot-Moss et al., 2010). Conversely, LSF2 binds and dephosphorylates glucans, but it is notable that this glucan phosphatase lacks a CBM (Santelia et al., 2011). Indeed, the glucan phosphatase family was first defined as any protein containing both a DSP and CBM (Gentry et al., 2007). Thus, the physical basis for LSF2–starch interaction and dephosphorylation is unclear, although it has been previously suggested that LSF2 may use a scaffold protein or an unidentified glucan binding interface to maintain interactions with starch (Comparot-Moss et al., 2010; Santelia et al., 2011).

Here, we elucidate the functional basis for LSF2 as a specific glucan phosphatase by determining the x-ray crystal structure of LSF2 with and without the phospho-glucan products maltohexaose and phosphate. LSF2 possesses a unique DSP active site that incorporates both a glucan binding platform and phosphatase catalytic residues. Moreover, we identify two additional secondary binding sites (SBSs) located >20 Å from the active site that intimately involve the CT motif and are essential for LSF2 glucan binding and dephosphorylation, providing the distinct mechanism necessary for LSF2 to function without a CBM.

RESULTS

Crystal Structure of LSF2 Bound to Maltohexaose and Phosphate

The structure of the *Arabidopsis* LSF2 glucan phosphatase (residues 79 to 282, C193S [catalytically inactive]) bound to maltohexaose and phosphate was determined to a resolution of 2.30 Å using molecular replacement with one molecule in the asymmetric unit (Figure 1A, Table 1). The LSF2 DSP domain (residues 79 to 244) possesses a characteristic core PTP fold consisting of a central five-stranded β-sheet region flanked by eight α-helices (see Supplemental Figure 1 online). The CT motif (residues 245 to 282) consists of a loop region culminating in an α-helix that integrally folds into the DSP domain, a characteristic also found in the glucan phosphatase SEX4 (Vander Kooi et al., 2010). A search for structural homologs of the LSF2 DSP domain (residues 79 to 244) identified the DSP domain of *Arabidopsis* SEX4 (residues 90 to 250, root mean square deviation [RMSD] of 1.1 Å, PDB code 3NME; Vander Kooi et al., 2010) and mouse PTPMT1 (residues 105 to 256, RMSD of 2.2 Å, PDB code 3RGQ; Xiao et al., 2011) as the structures most similar to LSF2 despite the fact that the LSF2 DSP is only 48 and 17% identical at the amino acid level to the DSP domain of SEX4 and PTPMT1, respectively.

Maltohexaose is composed of six Glc moieties with α-1,4-glycosidic linkages; thus, it is similar to the unwound helices on the starch granular surface. In the structure, maltohexaose is bound to the LSF2 active site and two distal sites. The LSF2 active-site region contains a single maltohexaose chain and phosphate molecule within the catalytic pocket. Multiple conserved DSP active-site motifs converge to form an extended active-site binding pocket within LSF2 that is ~19Å long and ~9Å deep with 511 $Å^2$ contact area (Figure 1B). These motifs include a recognition domain from α1 through β1 (83 to 92), a variable (V-) loop from α3 through α4 (132 to 150), a WPD (D-) loop between β4 and α5 (158 to 163), a PTP-loop between β5 and α6 (192 to 199) that contains the LSF2 catalytic signature (Cx_5R) motif, and an R-motif between α7 and α8 (225 to 244) (see Supplemental Figures 1 and 2 online).

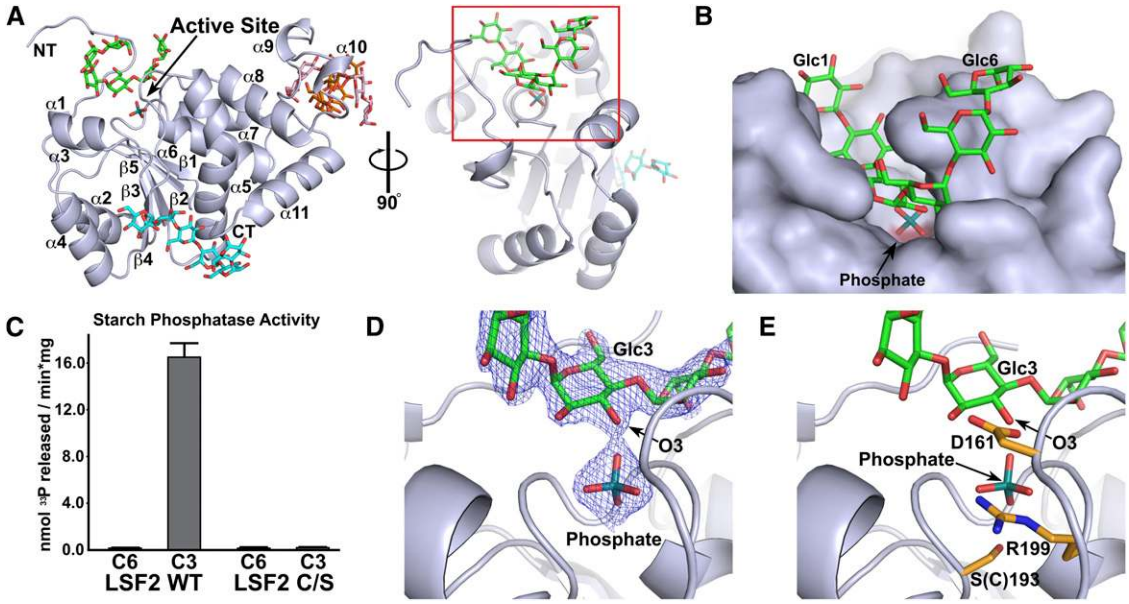

Figure 1. Structure of LSF2 Bound to Maltohexaose and Phosphate.

(A) Ribbon diagram of LSF2 (residues 79 to 282, C193S). Maltohexaose chains (green, cyan, orange, and pink) and phosphate (teal) are shown. Elements of secondary structure are numbered consecutively from N to C termini.

(B) Maltohexaose chain (green) and phosphate (teal) at the active-site (red) channel. Image correlates with the red box in **(A)**. Glc moieties are numbered from the nonreducing to the reducing end. The total contact area of the active-site channel with phosphate and maltohexaose is 511 Å^2.

(C) Specific activity of LSF2 wild type (WT) and inactive mutant LSF2 C193S (C/S) against the C6- and C3-position of *Arabidopsis* starch. Phosphate-free starch was purified from *gwd*-deficient *Arabidopsis* (Yu et al., 2001), and the starch was prelabeled with ^{33}P at either the C6- or C3-position and then incubated with recombinant protein. Starch dephosphorylation over time was linear and was measured via release of ^{33}P. The reaction time was 5 min. Each bar is the mean + SD of six replicates.

(D) 2Fo-Fc electron density map of maltohexaose chain (green) and phosphate (teal) at the active site (1.35 σ). The O3 group of Glc3 is highlighted.

(E) LSF2 active-site catalytic triad (yellow) residues interact with maltohexaose and phosphate. S(C)193 (catalytically inactive mutant, C193S) and R199 are located within the PTP-loop between β5 and α6, and Asp-161 is located within the D-loop between β4 and α5.

LSF2 C3 Specificity and Catalytic State

LSF2 possesses robust activity against starch and displays high specificity for the C3 position, as measured by a ^{33}P-radiolabeled starch dephosphorylation assay (Figure 1C) (Santelia et al., 2011). While both glucan dikinases and glucan phosphatases display strong positional specificity, the basis of this specificity is unclear. The electron density of the maltohexaose in the active site allows clear assignment of glucan chain position and orientation, labeled Glc1-Glc6 from the nonreducing end to the reducing (Figure 1D; see Supplemental Figures 3A and 3B online). Strikingly, the O3 group of Glc3 directly interacts with the phosphate at the LSF2 catalytic site at a distance of 2.4 Å compared with 7.0 Å for the O6 group. Furthermore, the orientation of the PTP catalytic triad (**D**X_{30-35}**C**X_5**R**) within LSF2 is proximal to the O3 and phosphate and poised for catalysis of a C3-phosphorylated Glc (Figure 1E). C193S is located at the base of the active-site cleft, 2.5 Å from the nearest phosphate oxygen, and represents the key nucleophilic catalytic residue that covalently attacks the phosphate group during catalysis. Arg-199 is positioned 2.8 Å from the phosphate and orients the phosphate of the substrate toward the catalytic Cys. At the top of the active-site cleft is the D-loop Asp-161 that participates in catalysis as a general acid/base, forming the reaction intermediate and then assisting in hydrolysis and product expulsion. Asp-161 is located 2.5 Å from the O3 of Glc3 and 3.8 Å from the nearest phosphate oxygen.

Maltohexaose-Phosphate Product Bound at the LSF2 Active Site

Five highly conserved aromatic residues delineate the boundaries of the extended active-site channel, forming extensive interactions with the Glc rings of the maltohexaose chain (Figure 2A). These five aromatic residues provide the majority of the interface between the LSF2 active site and the substrate. Tyr-83, Tyr-85, Tyr-135, and Trp-136 form one side of the channel and interact with Glc moieties Glc1-5. Tyr-83 and Tyr-85 are located within the recognition domain, directly adjacent to the R-motif and PTP-loop, respectively. Tyr-135 and Trp-136 are both located in the V-loop and form a continuous interaction surface with Tyr-85. Phe-162, located in the D-loop, forms the opposite side of the aromatic channel and interacts with Glc2-6. These Glc moieties form a helical structure around Phe-162 and interact with both faces of the Phe ring. The residues that form the aromatic channel are strictly conserved in all land plants as well as in most single-celled members of Kingdom Plantae, with only one

Table 1. Crystallographic Statistics

Crystal	Δ78-LSF2 C193S: Maltohexaose, Phosphate	Δ78-LSF2 Wild Type: Citrate
PDB code	4KYR	4KYQ
Data collection		
Space group	$P6_522$	$P2_12_12$
Cell dimensions		
a, *b*, *c* (Å)	92,78, 92.78, 144.94	51.82, 99.58, 37.76
α, β, γ (°)	90, 90, 120	90, 90, 90
Wavelength (Å)	1.00	1.00
Resolution range (Å) (highest shell resolution)	20.0-2.30 (2.38-2.30)	20.0-1.65 (1.71-1.65)
R_{merge} (highest shell)	10.8 (39.1)	6.6 (59.3)
$I/\sigma I$ (highest shell)	9.0 (2.2)	20.5 (2.3)
Completeness (%) (highest shell)	94.8 (87.3)	90.1 (86.3)
Redundancy (highest shell)	3.7 (2.5)	4.7 (4.7)
Refinement		
Resolution (Å)	2.30	1.65
No. reflections	15288	20833
R_{work}/R_{free}	17.4/22.9	15.7/19.9
No. atoms		
Protein	1685	1711
Ligand/ion	251	13
Water	88	161
B-factors		
Protein	45.4	19.8
Ligand/ion	37.6 (phosphate) 70.1 (maltohexaose, active site) 59.1 (maltohexaose, Site-2) 60.8 (maltohexaose, Site-3, hex-1) 86.1 (maltohexaose, Site-3, hex-2)	14.6 (citrate)
Water	49.7	31.5
RMSDs		
Bond lengths (Å)	0.014	0.014
Bond angles (°)	2.1	1.7
Ramachandran plot		
Most favored regions (%)	97.6	97.7
Additional allowed regions (%)	2.4	2.3
Disallowed regions (%)	0.0	0.0

nonconservative substitution (*Volvox carteri* L83; see Supplemental Figure 2 online).

To investigate the functionality of these aromatic residues, we generated Ala mutants of each channel residue and tested their ability to dephosphorylate starch granules isolated from *Arabidopsis*. Single Ala point mutations of Tyr-83, Tyr-85, Tyr-135, Trp-136, and Phe-162 resulted in a decrease of C3-dephosphorylation by 38 to 96% (Figure 2B). Mutation of both sides of the channel (W136A/F162A) resulted in a 99% loss of glucan phosphatase activity. Importantly, the observed decreases in specific glucan phosphatase activity were not due to destabilization of the active site or misfolding of the protein as evidenced by near-wild-type phosphatase activity for all mutant proteins toward the generic substrate *para*-nitrophenyl phosphate (pNPP) (see Supplemental Figure 4A online). Thus, our findings indicate that LSF2 possesses an aromatic channel that forms an extended active site uniquely suited to bind to polyglucan substrates and necessary for glucan phosphatase activity.

Conformational Changes in the LSF2 Active Site

Intriguingly, one of these key aromatic residues, Phe-162, is found in the D-loop directly after Asp-161, which serves as the general acid/base as discussed above. In fact, Phe-162 makes the most contact of any active-site residue with the substrate glucan (136 Å^2, 27% of the total contact area). To compare the catalytic site of glucan-bound and unbound LSF2, we crystallized LSF2 without maltohexaose and determined the structure to a resolution of 1.65 Å using molecular replacement (see Supplemental Figure 5 online; Table 1). The glucan-free LSF2 produced a different crystal form and contained one molecule in the asymmetric unit and bound citrate from the crystallization buffer (see Supplemental Figure 5 online). The RMSD of the glucan and citrate-bound DSP domain (residues 79 to 244) structures was 1.0 Å. A comparison of product-bound and citrate-bound LSF2 structures revealed a substrate-dependent rearrangement of the D-loop architecture upon glucan binding (Figure 2C). In the product-bound structure, the orientations of Asp-161 and Phe-162 are significantly different. The D-loop aromatic residue Phe-162, important for the specific activity of LSF2, interacts with multiple Glc moieties of the glucan chain and shifts toward the V-loop. This movement is associated with a significant reorientation of the critical general acid/base, residue Asp-161. Comparison of the two structures reveals that the terminal carboxylate of Asp-161 is 3.1 Å closer to the catalytic Cys and directly in contact with the O3 group of Glc3. To further analyze the position of Asp-161, we compared the LSF2 DSP with structures of the glucan phosphatase SEX4 and the prototypical protein phosphatases VHR (PDB 1VHR; Yuvaniyama et al., 1996) and SSH-2 (PDB 2NT2; Jung et al., 2007). Analysis of the catalytic triad from each of these structures reveals that the substrate-bound orientation of LSF2 Asp-161 is in a catalytically competent orientation only in the product-bound structure (see Supplemental Figure 6 online). Thus, LSF2 undergoes a substrate-induced conformational change with the LSF2 product-bound form ideally positioned for catalysis of an O3 phosphorylated glucan substrate.

Most DSPs possess a short-chain hydrophilic reside, S/T/N/H, at the +1 residue from the general acid/base Asp (Vander Kooi et al., 2010). However, Phe-162 is invariant in LSF2, and the corresponding residue is also strictly conserved in SEX4, Phe-167. We previously demonstrated that mutating SEX4 Phe-167 to a short-chain hydrophilic residue (F167S) resulted in a 50% decrease in the glucan/pNPP phosphatase activity of SEX4 F167S (Vander Kooi et al., 2010). Cumulatively, these data demonstrate an important role for D-loop movement in order to correctly position the catalytic triad and maximize glucan phosphatase activity.

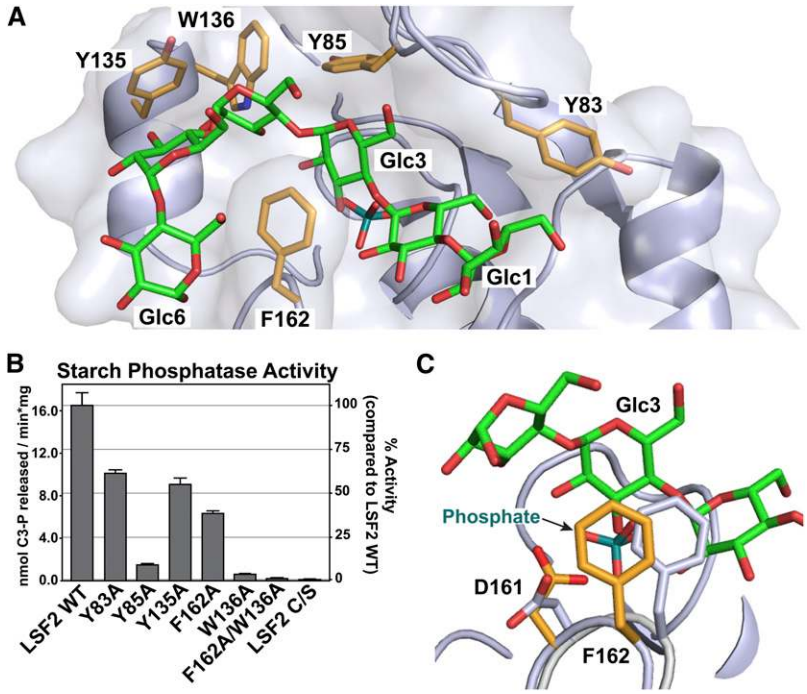

Figure 2. The LSF2 Aromatic Channel.

(A) A maltohexaose chain (green) interacts with aromatic channel residues at the LSF2 active site. Tyr-83 and Tyr-85 are located in the recognition domain N terminus from α1. Tyr-135 and Trp-136 are located in the V-loop in α3. Phe-162 is located in the D-loop between β4 and α5. The total contact area of the aromatic channel residues with maltohexaose is 266 Å^2.

(B) Specific activity of aromatic channel mutants against the C3-position of *Arabidopsis* starch granules. Phosphate-free starch from *gwd*-deficient plants (Yu et al., 2001) was purified and prelabeled at the C3- or C6-position with ^{33}P as in Figure 1C. The labeled starch was then incubated with LSF2 wild type (WT) or LSF2 aromatic channel mutants, and starch dephosphorylation was measured via release of ^{33}P. The reaction time was 5 min. Each bar is the mean + SD of six replicates. Mutated residues are marked with an asterisk in Supplemental Figure 2 online.

(C) Substrate-dependent positional rearrangement of the D-loop. D-loop residues Phe-162 (aromatic channel) and Asp-161 (catalytic residue) lie between β4 and α5 and undergo significant movement in the maltohexaose/phosphate bound (blue/yellow) versus the unbound (gray/blue) LSF2 structures.

Noncatalytic Glucan Binding Sites

Glucan phosphatases were originally defined as enzymes that contain both a DSP and CBM domain, and the CBM has been shown to be critical for endogenous substrate binding and biological activity (Gentry et al., 2007; Gentry and Pace, 2009). Because LSF2 lacks a CBM, the nature of its substrate binding ability has been unclear. Therefore, we investigated LSF2 glucan binding to amylopectin. LSF2 was incubated with amylopectin, and the amylopectin was then pelleted by ultracentrifugation. Proteins in the pellet and supernatant were separated by SDS-PAGE and visualized by immunoblot analysis. The prototypical protein phosphatase VHR does not bind amylopectin and was found in the supernatant, whereas the prototypical glucan phosphatase SEX4 possesses robust glucan binding and was largely in the pellet (Figure 3A). LSF2 also robustly binds amylopectin and similar to SEX4 was largely in the pellet. Next, we sought to define how mutations in the aromatic channel affect LSF2 glucan binding. The LSF2 W136A/F162A mutant, which had a 99% decrease in specific glucan phosphatase activity, showed only a moderate (32%) decrease in amylopectin binding (Figure 3A). This suggests that while the active site is necessary for glucan phosphatase activity, other regions primarily determine substrate binding. These data are consistent with LSF2 containing additional glucan binding sites distinct from the active-site aromatic channel.

Indeed, the maltohexaose-bound LSF2 structure revealed two additional glucan binding sites >20 Å from the active site (Figure 3B). Thus, we hypothesized that one or both of these additional glucan binding sites could functionally replace a CBM domain and be critical for the biological activity of LSF2.

One maltohexaose chain is located in a binding pocket (Site-2) formed by residues from the DSP domain and CT motif on the opposite side of the V-loop ~21 Å from the active site. The maltohexaose chain makes extensive contacts (391 Å^2) with residues in β4 and α5 of the DSP as well as the C terminus of the CT domain (Figure 4A; see Supplemental Figures 3C and 3D online). The maltohexaose chain wraps around the CT-loop, forming hydrogen bonds with Arg-153 and Arg-157 and van der Waals contact with Trp-180 and Met-155. As with the active-site residues, Site-2 residues are highly conserved in LSF2 orthologs (see Supplemental Figure 2 online). To determine the effect of

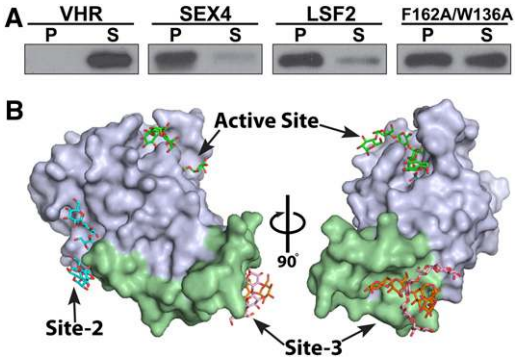

Figure 3. LSF2 Glucan Binding Sites.

(A) Results from cosedimentation assay of protein and amylopectin (amylopectin binding assay). Recombinant His-tagged proteins were incubated with 5 mg/mL amylopectin, amylopectin was pelleted by ultracentrifugation, and proteins in the pellet (P) and supernatant (S) were separated by SDS-PAGE and visualized by immunoblot analysis. Amylopectin-bound proteins are found in the pellet and unbound proteins are found in the supernatant.

(B) Surface model of LSF2 showing DSP domain (blue) and CT motif (green). Maltohexaose chains at the active site (green), Site-2 (cyan), and Site-3 (orange and pink) are shown.

Site-2 glucan binding on LSF2 activity, we tested the ability of Ala point mutants as well as a C-terminal truncation to dephosphorylate starch granules. Ala mutations of Trp-180, Met-155, Arg-153, and Arg-157 resulted in decreases of specific glucan phosphatase activity of 24 to 50% (Figure 4B). Truncation of the three C-terminal residues (R280/G281/T282, ΔRGT) decreased activity by 46%. All mutant proteins maintained near-wild-type pNPP activity, indicating that the observed effects are specific (see Supplemental Figure 4B online). While mutation of Site-2 resulted in a substantial decrease in glucan phosphatase activity, we also investigated the effect of Site-2 mutants on substrate binding. We tested the ability of LSF2 R157A, which showed the greatest reduction in specific activity, to bind amylopectin and found that it displayed a substantial (64%) decrease in amylopectin binding (Figure 4C). This decrease was markedly greater than that observed for the W136A/F162A active-site mutant (Figure 3A). These data demonstrate that Site-2 functions as a glucan binding interface and that this binding site is important for the biological activity of starch dephosphorylation by LSF2.

Two additional maltohexaose chains were found in a binding pocket (Site-3) formed by the CT-loop region ~23 Å from the active site. Five Glc moieties from two maltohexaose chains (Hex-1 and Hex-2) could be resolved (Figure 5A; see Supplemental Figures 3E and 3F online). The two chains form a helical structure, reminiscent of an amylopectin helix, with a contact area of 338 Å^2. LSF2 primarily interacts with Hex-1, forming hydrogen bonding interactions with Lys-245 and Glu-268 and van der Waal's interactions with Phe-261. As with the active-site and Site-2 residues, Site-3 residues are highly conserved in LSF2 orthologs (see Supplemental Figure 2 online). To determine the effect of Site-3 glucan binding on LSF2 activity, we tested the ability of Ala point mutants to dephosphorylate starch granules. Ala mutations of Glu-268, Lys-245, and Phe-261 resulted in decreases of specific glucan phosphatase activity of 35 to 87% (Figure 5B). All mutant proteins maintained near-wild-type pNPP activity, again indicating that the observed effects are specific (see Supplemental Figure 4C online). As with Site-2, we also investigated the effect of Site-3 on substrate binding. We found that the Site-3 mutant F261A, which showed

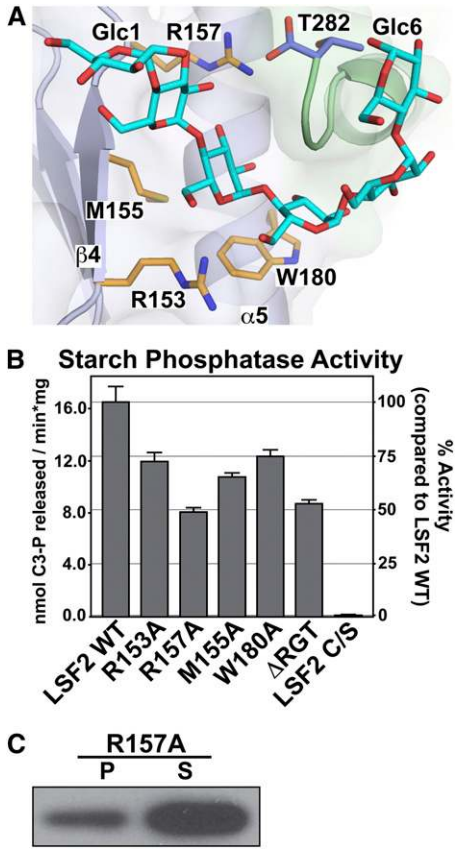

Figure 4. LSF2 Glucan Binding Site-2.

(A) A transparent surface model of LSF2 Site-2 showing DSP domain (blue) and CT motif (green) interaction with the maltohexaose chain (cyan). Arg-153 and Met-155 are located on β4. Arg-157 is located between β4 and α5. Trp-180 is located on α5. Thr-282 is located on the C terminus after α11. Glc moieties are numbered from nonreducing to reducing end. The total contact area of Site-2 with maltohexaose is 391 Å^2.

(B) Specific activity of Site-2 mutants against the C3-position of *Arabidopsis* starch granules. Phosphate-free starch from *gwd*-deficient plants (Yu et al., 2001) was purified and prelabeled at the C3- or C6-position with ^{33}P as in Figure 1C. The labeled starch was then incubated with LSF2 wild type (WT) or LSF2 Site-2 mutants, and starch dephosphorylation was measured via release of ^{33}P. In addition to single point mutants, starch dephosphorylation was also determined for LSF2 lacking the C-terminal residues Arg-280, Gly-281, and Thr-282 (ΔRGT). The reaction time was 5 min. Each bar is the mean + SD of six replicates. Mutated residues are marked with a circle in Supplemental Figure 2 online.

(C) An amylopectin binding assay of Site-2 mutant R157A was performed in a similar manner as described in Figure 3A. LSF2 R157A was cosedimented with amylopectin and found in the pellet (P) and supernatant (S).

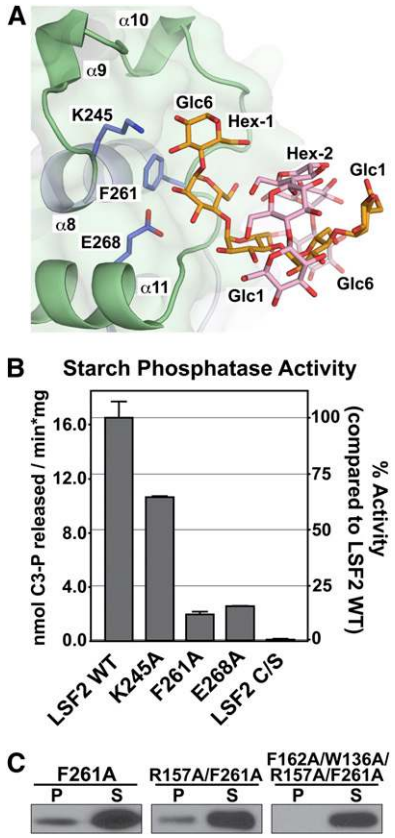

Figure 5. LSF2 Glucan Binding Site-3.

(A) A transparent surface model of LSF2 at the CT motif loop (green) showing specific interactions with maltohexaose chains Hex-1 (orange) and Hex-2 (pink). Lys-245 is located between α8 and α9. Phe-261 is located between α10 and α11. Glu-268 is located in α11. The total contact area of Site-3 with the maltohexaose chains is 338 Å^2.

(B) Specific activity of Site-3 mutants against the C3-position of *Arabidopsis* starch granules. Phosphate-free starch from *gwd*-deficient plants (Yu et al., 2001) was purified and prelabeled at the C3- or C6-position with ^{33}P as in Figure 1C. The labeled starch was then incubated with LSF2 wild type (WT) or LSF2 Site-3 mutants, and starch dephosphorylation was measured via release of ^{33}P. The reaction time was 5 min. Each bar is the mean + SD of six replicates. Mutated residues are marked with a triangle in Supplemental Figure 2 online.

(C) An amylopectin binding assay of Site-3 mutant F261A, Site-2/Site-3 mutant (R157A/F261A), quadruple mutation of active site, Site-2, and Site-3 (F162A/W136A/R157A/F261A) was performed in a similar manner as described in Figure 3A. Amylopectin-bound protein is found in the pellet (P) and unbound protein is found in the supernatant (S).

the greatest reduction in specific activity, showed the most dramatic (73%) decrease in amylopectin binding (Figure 5C). In comparison to Site-2, Site-3 mutants showed greater effects on both substrate binding and specific glucan phosphatase activity.

To determine the contribution of the individual glucan binding sites to the overall binding of LSF2, we generated combination mutants. The combination of Site-2 and Site-3 mutations, R157A/F261A, led to an even more dramatic (87%) decrease in amylopectin binding, but slight binding still remained (Figure 5C). Only a mutant combining all three sites, F162A/W136A/R157A/F261A, resulted in a protein that possessed no detectable glucan binding ability (Figure 5C). Thus, each of the three glucan binding sites contributes to substrate binding, and none of the sites are individually sufficient for wild-type levels of glucan binding. In addition, all of the LSF2 residues directly involved in noncatalytic glucan binding are not conserved in the CBM-containing SEX4 (see Supplemental Figure 7 online). Taken together, these data demonstrate that rather than requiring a scaffold protein or CBM, LSF2 possesses three glucan binding sites in its DSP domain that are each critical for its ability to bind glucans and function as a specific glucan phosphatase.

DISCUSSION

Phosphatases dephosphorylate each of the four organic macromolecules: proteins, lipids, nucleic acids, and carbohydrates. While previous studies have defined the structural bases of phosphatase activity with proteins, lipids, and nucleic acids, the basis for phosphatase–glucan interaction was previously unknown. Here, we examined the structural and biochemical basis of glucan phosphatase activity by determining the crystal structure of LSF2, providing detailed insights into the mechanism of this important class of enzymes.

At the LSF2 active site, an integrated network of aromatic residues forms an extended binding pocket that allows specific glucan interaction and dephosphorylation. While these aromatic residues are within the core DSP domain, in each case they are uniquely suited to promote phospho-glucan binding. Conservation of aromatic residues in the active site between glucan phosphatases suggests that this is a key general characteristic differentiating glucan phosphatases from other phosphatases. It is particularly notable that both LSF2 and the previously determined SEX4 structure possess an α-helical V-loop containing conserved aromatic residues, Tyr-135 and Trp-136 in the LSF2 V-loop (Vander Kooi et al., 2010). These residues are integral for LSF2 glucan binding and dephosphorylation and form the basis of the conserved theme of an aromatic channel within the active site of glucan phosphatases. By contrast, the V-loop of PTPs and DSPs are historically defined by their lack of secondary structure and highly variable length (Alonso et al., 2003). Phospho-Tyr phosphatases contain longer V-loops when compared with phospho-Ser/Thr phosphatases in order to generate a deeper binding pocket that accommodates the longer phospho-Tyr. However, in each case, the V-loop is indeed a loop (Alonso et al., 2003; Tonks, 2006). Thus, the glucan phosphatase structured V-loop appears to be a defining characteristic of this phosphatase class.

Aromatic-Glc stacking interactions are a central structural element for CBMs (Boraston et al., 2004; Machovic and Janecek, 2006) and are found in the catalytic channel of glycosyl hydrolases (Robert et al., 2005; Koropatkin and Smith, 2010). However, a similar glucan-aromatic channel interface had not been previously observed in any phosphatase. Our crystallography data revealed that the LSF2 active site maintains interactions with all six Glc moieties on the maltohexaose chain, thus indicating that the active site of LSF2 combines both a DSP active site and glucan binding platform.

Indeed, we identified a link between LSF2 substrate binding and catalysis mediated by residue Phe-162. In addition to being a part of the active-site aromatic channel, Phe-162 is located at the +1 position from the catalytic triad residue Asp-161. Rotation of these residues upon glucan binding is required for the correct catalytic positioning of Asp-161. This connection suggests an inherent mechanism for phosphate recognition that is tied directly to the architecture of the glucan phosphatase aromatic channel. It is important to note that this may be a general feature of this enzyme class since this residue is conserved as an aromatic/long-chain hydrophobic residue in all known glucan phosphatases, whereas other phosphatases typically possess short-chain hydrophilic residues at this position (Vander Kooi et al., 2010).

Despite similarities with other glucan phosphatases, LSF2 is in fact unique among known glucan phosphatases in that the enzyme functions independent of a CBM. There has been debate as to whether or not other functionality or possibly bridging proteins are required for the glucan phosphatase activity of LSF2 (Comparot-Moss et al., 2010; Santelia et al., 2011). However, our data clearly establish that LSF2 uses three glucan binding sites located in the phosphatase domain for carbohydrate binding. The central function attributed to CBMs is substrate localization, and our data demonstrate that the noncatalytic glucan binding sites identified in the LSF2 structural data adopt this functionality. Mutations of Site-2 and Site-3, the two binding sites located away from the active site, result in dramatic decreases in LSF2 glucan binding and dephosphorylation, similar to decreases observed for CBM mutants of SEX4 and laforin (Ganesh et al., 2004; Wang and Roach, 2004; Gentry et al., 2007). It should be noted that Site-2 and Site-3 both use residues from the glucan phosphatase–specific CT motif (Vander Kooi et al., 2010; Santelia et al., 2011). Thus, this unique elaboration on the core LSF2 phosphatase domain provides novel functionality.

Carbohydrate active enzymes (CAZymes) as defined by the CAZy database (http://www.cazy.org) are a diverse collection of enzymes that synthesize and degrade an extremely heterogeneous group of complex carbohydrates and glycoconjugates (Cantarel et al., 2009). These enzymes cover >250 protein families, including glycoside hydrolases, glycosyltransferases, polysaccharide lyases, carbohydrate esterases, and nonenzymatic proteins that contain a CBM (Cantarel et al., 2009). A CBM is a contiguous amino acid sequence with a conserved tertiary fold that possesses carbohydrate binding ability and is contained within a carbohydrate-modifying enzyme (Coutinho and Henrissat, 1999; Boraston et al., 2004; Machovic and Janecek, 2006; Cantarel et al., 2009). Many of the enzymes that synthesize and degrade carbohydrates utilize a CBM to bind their carbohydrate substrate and then enzymatically act on the carbohydrate via a distinct catalytic module. This model of a binding domain and enzymatic domain is true for the other identified glucan phosphatases (Worby et al., 2006; Gentry et al., 2007; Kötting et al., 2009; Vander Kooi et al., 2010). Indeed, the glucan phosphatases were originally defined as any protein containing a phosphatase domain and a CBM (Gentry et al., 2007). While LSF2 is a carbohydrate-modifying enzyme that binds carbohydrates, it does not contain a classical CBM and is not classified under the CAZy classification.

Alternatively, LSF2 uses a glucan binding architecture referred to as secondary binding sites (SBSs) (Robert et al., 2005; Bozonnet et al., 2007; Cuyvers et al., 2012). SBSs are an emerging theme found in some glycoside hydrolases (Cuyvers et al., 2012). Many glycoside hydrolases possess one or more CBM, but recent structural studies have identified a subset of glycoside hydrolases that contain both a CBM and SBSs, such as SusG (Koropatkin and Smith, 2010), or that only possess SBSs, such as barley (*Hordeum vulgare*) α-amylase (Kadziola et al., 1998; Robert et al., 2005), human salivary and pancreatic α-amylase (Payan and Qian, 2003; Ragunath et al., 2008), and yeast glucoamylase (Sevcík et al., 2006). Indeed, the two SBSs of barley α-amylase, which are remote from its glucan binding active site, are directly involved in substrate binding and hydrolysis and these two sites act synergistically (Nielsen et al., 2009).

Our results establish that LSF2 independently binds and dephosphorylates starch. As starch is a complex, insoluble substrate, the presence of multiple glucan binding interfaces may permit LSF2 to uniquely engage the complex multivalent glucan

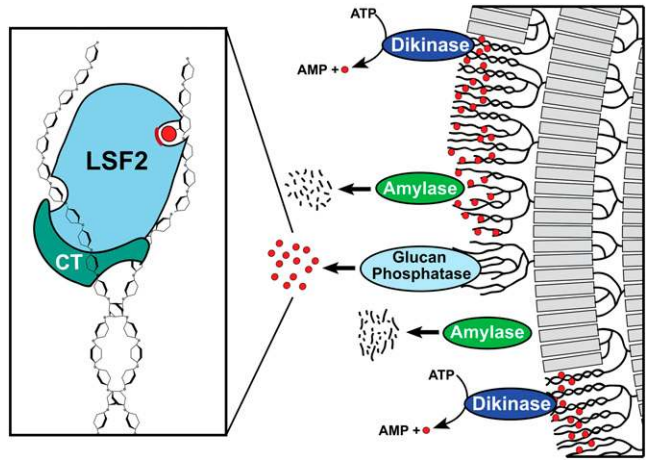

Figure 6. Proposed Model of Reversible Phosphorylation at the Starch Granular Surface during Breakdown (Modified from Streb and Zeeman, 2012).

At night, starch is phosphorylated (red circles) by glucan dikinases, leading to solubilization of the outer starch granules via unwinding of amylopectin helices (gray bars). Amylopectin is then hydrolyzed by amylases into maltose and malto-oligosaccharides. However, these amylases cannot completely degrade phosphorylated starch. Therefore, glucan phosphatases must remove phosphate from partially degraded amylopectin chains. The outer starch surface is then fully degraded by amylases into malto-oligosaccharides, and the cycle is reset so that the next starch layer can be phosphorylated and degraded. The inset box illustrates a model of LSF2-glucan interaction. Amylopectin helices are composed of two α-1,4-glycosidic–linked chains that are partially unwound at their nonreducing ends due to phosphorylation. LSF2 interacts with starch via multiple binding sites: The LSF2 active site (highlighted in red) interacts with the C3-phosphorylated Glc moiety through coordination of the aromatic channel with six Glc units, Site-2 also interacts with six Glc moieties via hydrogen bonding and van der Waals contacts at an interface between the LSF2 DSP domain (blue) and the CT motif (green), and Site-3 interacts with two helical-like glucan chains through interactions with the CT motif.

surface of its endogenous substrate. Indeed, the combined-site mutants (R157A/F261A and F162A/W136A/R157A/F261A) show additive effects, implying that the sites function together. This suggests a model whereby starch binding involves the engagement of longer or multiple glucan chains by the three glucan binding sites on LSF2 (Figure 6). Moreover, the helical glucan chains at Site-3 are reminiscent of amylopectin, suggesting LSF2 may interact with complex starch granules with distinct helical characteristics. The functional significance of SBSs in glycosyl hydrolases has been extensively reviewed and various additional functions have been postulated, including substrate disruption, allosteric regulation, enhancing processivity, and relaying of reaction products (Cuyvers et al., 2012). Due to the limitations of using the short-chain glucan maltohexaose as a ligand, ongoing studies using more diverse glucan chains will be required to examine possible cooperativity or connectivity between the additional LSF2 glucan binding sites. This may also provide insights into the position of LSF2 binding and C3-phosphorylation relative to amylopectin branch points.

These data also give a clearer picture of the role of glucan phosphatases in the cyclical starch degradation process. The glucan dikinases phosphorylate the outer Glc moieties of starch at the C6- and C3-positions, resulting in amylopectin helix unwinding and local solubilization. These events allow α- and β-amylases as well as isoamylases to access the outer glucans and release maltose and malto-oligosaccharides. However, β-amylase activity is inhibited when a phosphate group is reached. The glucan phosphatases bind and dephosphorylate the phospho-glucans to allow further amylolytic activity and a resetting of the starch degradation cycle (Figure 6). The coordinated phosphorylation of starch Glc at the C6- and C3-positions is the central signaling event orchestrating starch breakdown (Blennow and Engelsen, 2010; Kötting et al., 2010; Streb and Zeeman, 2012). The recent characterization of SEX4 and LSF2 illustrates that plants use a two-enzyme system for phosphate removal, permitting complete starch catabolism. Our structures reveal the basis for the glucan binding and C3-specificity of LSF2. Determination of additional glucan phosphatase structures will reveal further insights into the mechanism of activity and specificity of glucan phosphatases. In particular, it will be interesting to determine if the presence of a CBM domain in other family members not only contributes to substrate binding but also to position-specific function.

As the central regulatory event governing starch breakdown, modulation of reversible phosphorylation has the potential to increase starch yields and produce starches with novel physicochemical properties, thus enhancing manufacturing of feedstock for both food and nonfood applications (Santelia and Zeeman, 2011). Starch is used in countless applications, many of which require chemical and physical modifications to improve and diversify its functionality (Blennow et al., 2002; Santelia and Zeeman, 2011). Phosphorylation is the only known natural modification of starch, and highly phosphorylated starches have many attractive characteristics, including increased hydration status (Muhrbeck and Eliasson, 1991), decreased crystallinity (Muhrbeck and Eliasson, 1991), and improved freeze-thaw stability, viscosity, and transparency (Blennow et al., 2001). *Arabidopsis* plants lacking LSF2 activity display increased C3-phosphorylated starch without adverse effects on plant growth (Santelia et al., 2011). Genetic manipulation of LSF2 could therefore represent a new means to produce starch with higher phosphate content, particularly in cereal crops containing virtually no covalently bound phosphate (Blennow et al., 2000). The data presented here can be used to inform the engineering of glucan phosphatases to alter their functionality for industrial starch processing, particularly in light of disparities between C6- and C3-contributions to starch superstructure. It has been established that C3-phosphorylation results in greater local hydration of starch granules compared with C6-phosphorylation; therefore, manipulation of LSF2 represents a potential avenue for manipulation of overall starch structure (Blennow and Engelsen, 2010). Structural insights into the unique mechanism of LSF2 are fundamental to our understanding of starch catabolism and ultimately harnessing starch as a biomolecule with diverse applications.

METHODS

Cloning, Expression, and Purification of Recombinant Proteins

Primers used in this work are listed in Supplemental Table 1 online. Cloning of full-length *Arabidopsis thaliana* LSF2 (AT3G10940) from cDNA was previously described (Santelia et al., 2011). Based on data from secondary structure predictions, disorder predictions, sequence similarity to SEX4, and analysis of LSF2 orthologs, we generated an *Arabidopsis* LSF2 construct lacking the first 78 amino acids (Δ78-LSF2). Δ78 LSF2 does not contain the chloroplast targeting peptide (predicted to be residues 1 to 65) along with residues up to the DSP recognition domain. Δ78-LSF2 was subcloned into pET28 (Novagen) using *Nde*I and *Xho*I sites to encode a His_6 tag, a thrombin cleavage site, and Δ78-LSF2 (Santelia et al., 2011). We generated an active-site Cys-to-Ser mutation (C193S), an established technique that generates a catalytically inactive construct used to trap the substrate and as a negative control in enzymatic assays (Zhou et al., 1994; Jia et al., 1995; Begley et al., 2006). All point mutants were generated using a site-directed mutagenesis kit (Agilent) or mutagenesis services (GenScript). Cloning and purification of *Arabidopsis* SEX4 lacking the first 89 amino acids (Δ89-SEX4) (Vander Kooi et al., 2010) and *Hs*-VHR (Yuvaniyama et al., 1996) was performed as previously described. All DNA sequencing (ACGT) was confirmed using MacVector. Amino acid sequences of LSF2 orthologs were aligned with ClustalW in MacVector. Expression and purification of Δ78-LSF2 was performed similarly to the previously described method for Δ89-SEX4 (Vander Kooi et al., 2010). Briefly, BL21-CodonPlus *Escherichia coli* cells were transformed with expression vectors for the production of native LSF2 protein. Cells were grown at 37°C in 2× YT media to OD_{600} = 0.6 to 0.8, placed on ice for 20 min, induced with 1 mM isopropyl β-D-thiogalactoside, grown at 16°C for 16 h, and harvested by centrifugation. Cells were lysed in 20 mM Tris-HCl, pH 7.5, 100 mM NaCl, and 2mM DTT and centrifuged, and the proteins were purified via a Profinia IMAC Ni^{2+} column (Bio-Rad) with a Profinia protein purification system (Bio-Rad). Protein was dialyzed in 20 mM Tris-HCl, pH 7.5, 100 mM NaCl, and 2mM DTT overnight at 4°C in the presence of thrombin. Affinity purified protein was then reverse purified over the Profinia IMAC Ni^{2+} column, and the flow-through fraction was collected. Protein was further purified to homogeneity using a HiLoad 26/60 Superdex 200 size exclusion column (GE Healthcare). Protein used for enzyme and binding assays was stored in 10% glycerol as a cryoprotectant and flash frozen for later use.

Recombinant potato (*Solanum tuberosum*) GWD and recombinant *Arabidopsis* PWD for ^{33}P labeling of *Arabidopsis* starch were purified as previously described with the following modifications (Ritte et al., 2002; Kötting et al., 2005). GWD and PWD were transformed into BL21-

CodonPlus *E. coli* cells and expressed similarly to Δ78-LSF2 as stated above. GWD was lysed in buffer (50 mM Tris/HCl, pH 7.5, 2.5 mM EDTA, 2.5 mM DTT, and 0.5 mM PMSF), and proteins were purified using an anion exchange column (Q-sepharose-FF; GE-Healthcare) with a salt gradient (50 mM Tris/HCl, pH 7.5, 2.5 mM EDTA, 2.5 mM DTT, 0.5 mM PMSF, and 0.5 NaCl) to elute the protein. Fractions were collected and protein was further purified using a HiLoad 26/60 Superdex 200 size exclusion column (GE Healthcare) in new buffer (100 mM MOPS/KOH, pH 7.6, 1 mM EDTA, 2 mM DTT, 0.5 mM PMSF, and 150 mM NaCl). GWD was then put over a desalting column using a Bio-Scale Mini Bio-Gel P6 desalting column (Bio-Rad) using a Profinia protein purification system (Bio-Rad). PWD was lysed in buffer (50 mM HEPES/NaOH, pH 8.0, 300 mM NaCl, 10 mM imidazole, and 0.5 mM PMSF) and centrifuged, and proteins were purified using a Profinia IMAC Ni^{2+} column (Bio-Rad) with a Profinia protein purification system (Bio-Rad). PWD was further purified using a HiLoad 26/60 Superdex 200 size exclusion column (GE Healthcare).

Crystal Structure Determination and Refinement

For glucan-bound crystals, single, high-quality crystals with one molecule in the asymmetric unit were obtained via hanging drop vapor diffusion using a Mosquito liquid handling robot (TTPLabtech) using a 200-nL drop with a 1:3 ratio of Δ78-LSF2 C193S (4.8 mg/mL) preincubated with 25 mM maltohexaose (Sigma-Aldrich): 0.1 M diammonium hydrogen phosphate, pH 5.7, 17% 2-propoanol, and 31% polyethylene glycol 4000 at 18°C. Single, high-quality Δ78-LSF2 wild-type crystals, with one molecule in the asymmetric unit, were obtained with a 200-nL drop using a 1:1 ratio of LSF2 (4.8 mg/mL): 0.1 M trisodium citrate, pH 5.8, 16% 2-propanol, 31% polyethylene glycol 4000, and 2% glycerol at 18°C. A single crystal was used for data collection and structural determination for both LSF2 structures. Both Δ78-LSF2 C193S (phosphate/maltohexaose) and Δ78-LSF2 wild-type (citrate) data were collected on the 22-ID beamline of SER-CAT at the Advanced Photon Source, Argonne National Laboratory (Table 1) at 110K at a wavelength of 1.0 Å. Data were processed using HKL2000 (Otwinowski and Minor, 1997). PHENIX (Adams et al., 2010) was used for molecular replacement using the SEX4 DSP and α10 helix of the SEX4 CT domain as search models (Vander Kooi et al., 2010). The structures were then fully built and refined via iterative model building and refinement using Coot (Emsley et al., 2010) and Refmac5 (Murshudov et al., 1997), respectively. Stereochemistry of the model was analyzed using MolProbity (Davis et al., 2007). Analysis and molecular graphics were prepared using Pymol (Schrodinger, 2010). Density maps were produced using the FTT program in CCP4 (Winn et al., 2011). Comparative structure analyses were performed using the DaliServer (Holm and Rosenström, 2010) and DaliLite (Hasegawa and Holm, 2009). Protein-ligand contact analyses were performed with Areaimol (Lee and Richards, 1971).

Phosphatase Assays

Phosphatase assays using pNPP have been previously described and were performed with the following modifications (Worby et al., 2006; Gentry et al., 2007; Sherwood et al., 2013). Hydrolysis of pNPP was performed in 50 μL reactions, containing 1× phosphatase buffer (0.1 M sodium acetate, 0.05 M bis-Tris, 0.05 M Tris-HCl, pH 7.0, and 2 mM DTT), 50 mM pNPP, and 1 μg of enzyme at 37°C for 15 min. The reaction was terminated by the addition of 200 μL of 0.25 NaOH, and absorbance was measured at 410 nm. The assay was performed with each protein six times or more to determine specific activity.

Phosphate release from ^{33}P-Labeled granules was performed as previously described with the following variations (Hejazi et al., 2010; Santelia et al., 2011). C6-^{33}P-labeled starch was generated by isolating phosphate-free starch granules from the *Arabidopsis sex1-3* mutant (Yu et al., 2001), phosphorylating the starch with ^{33}P at the C6-position by GWD followed by washing until all unincorporated ^{33}P had been removed. Phosphorylation with unlabeled ATP at the C3-position by PWD was performed as previously described (Hejazi et al., 2010). C3-^{33}P-labeled starch was generated by isolating phosphate-free starch granules from the *Arabidopsis sex1-3* mutant (Yu et al., 2001), phosphorylating the starch with unlabeled ATP at the C6-position by GWD followed by phosphorylation with ^{33}P at the C3-position by PWD and washing until all unincorporated ^{33}P had been removed, as previously described (Hejazi et al., 2010). In both cases, the starch granules were phosphorylated at both positions; however, the ^{33}P-label was located at only one or the other position. [β-^{33}P]ATP was obtained from Hartmann Analytic. Recombinant proteins (150 ng) were incubated in dephosphorylation buffer (100 mM sodium acetate, 50 mM bis-Tris, 50 mM Tris-HCl, pH 6.5, 0.05% [v/v] Triton X-100, 1 μg/μL [w/v] BSA, and 2 mM DTT) with C6- or C3-prelabeled starch (4 mg/mL) in a final volume of 150 μL on a rotating wheel for 5 min at 25°C. The reaction was terminated by the addition of 50 μL of 10% SDS. The reaction tubes were then centrifuged at 13,000 rpm for 5 min to pellet the starch. ^{33}P release into 150 μL of supernatant was determined using a 1900 TR liquid scintillation counter (Packard). The assay was performed with each protein six times or more to determine specific activity.

Glucan Binding Assay

Glucan binding assays were performed as previously described with the following modifications (Gentry et al., 2007; Dukhande et al., 2011). All proteins used in the glucan binding assays were purified as described above without cleavage of the His_6 tag to maintain the epitope for immunoblot analysis. Amylopectin, from potato starch (Sigma-Aldrich) was solubilized by the Roach method (Wang and Roach, 2004) at a concentration of 5 mg/mL. Five milligrams of amylopectin was then prepelleted via centrifugation at 110,000*g* for 1.5 h at 4°C to collect only pelletable amylopectin and then resuspended in 0.5 mL binding buffer (50 mM Tris, 150 mM NaCl, pH 7.5, and 2 mM DTT). One microgram of recombinant protein was incubated in amylopectin solution for an hour at 4°C with rocking. The solution was then centrifuged at 110,000*g* for 1.5 h. Cosedimentation with amylopectin was measured by centrifuging the samples at 110,000*g* for 1.5 h. All supernatant was removed and protein was precipitated with 4 volumes of acetone stored at -20°C. Precipitated protein was then pelleted via centrifugation at 21,130*g* for 30 min, and excess acetone was removed using a SpeedVac concentrator (Savant) at 65°C for 1.25 h. Both soluble and pellet fractions were then resuspended in 30 μL RIPA buffer before the addition of 30 μL SDS-PAGE buffer (60 μL total volume for both the soluble and pellet fractions). Fifteen microliters of the pellet and soluble fraction were then resolved via SDS-PAGE, and relative concentration of pellet and soluble protein was analyzed by immunoblotting with α-His_6 antibody. Quantification of the signal was determined using ImageJ (Abramoff et al., 2004). The assay was performed three times or more with each protein to determine binding capacity.

Accession Numbers

Sequence data from this article can be found in the Arabidopsis Genome Initiative or GenBank/EMBL databases under the following accession numbers: LSF2, At3g10940; SEX4, At3g52180; GWD, At1g10760; PWD, At5g26570; and VHR, Hs03174. The atomic coordinates and structure factors have been deposited in the Protein Data Bank (PDB code 4KYR and 4KYQ, for maltohexaose/phosphate and citrate bound structures, respectively).

Supplemental Data

The following materials are available in the online version of this article.

Supplemental Figure 1. DSP Subdomains in LSF2.

Supplemental Figure 2. Conservation of LSF2 Orthologs.

Supplemental Figure 3. Electron Density Maps of Ligands in LSF2 Structure.

Supplemental Figure 4. Specific Activity of LSF2 and Mutants against *para*-Nitrophenyl Phosphate.

Supplemental Figure 5. Stereo View of Citrate at the LSF2 Active Site.

Supplemental Figure 6. Structural Alignment of the DSP Catalytic Triad of LSF2.

Supplemental Figure 7. Sequence Conservation of LSF2 and SEX4.

Supplemental Table 1. Sequences of Primers Used in This Work.

ACKNOWLEDGMENTS

We thank Samuel Zeeman and members of the Gentry and Vander Kooi labs for fruitful discussions as well as Carol Beach and Martin Chow in the Molecular Basis of Human Disease COBRE Proteomics Core and Protein Analytical Core, respectively, for technical assistance. This study was supported in part by an National Science Foundation CAREER Grant MCB-1252345 (M.S.G.), National Institutes of Health Grants R01NS070899 (M.S.G.) and P20GM103486 (M.S.G. and C.W.V.K.), Kentucky Science and Energy Foundation Grant KSEF-2268-RDE-014 (M.S.G.), a University of Kentucky Summer Research and Creativity Fellowship (T.M.B.), University of Kentucky College of Medicine startup funds (M.S.G.), the ETH-Zürich (O.K.), and Swiss-South African Joint Research Program Grant IZ LS X3122916 (D.S. and O.K.). The contents are solely the responsibility of the authors and do not necessarily represent the official views of the National Science Foundation, National Institutes of Health, or other funding agencies.

AUTHOR CONTRIBUTIONS

M.S.G., C.W.V.K., and D.A.M. designed the research. All authors performed research. C.W.V.K., D.A.M., H-.F.G., M.S.G., and S.H. analyzed data. D.A.M., C.W.V.K., and M.S.G. wrote the article, and D.A.M. generated the figures C.W.V.K. and M.S.G. contributed equally to the publication of this article.

Received April 16, 2013; revised May 31, 2013; accepted June 12, 2013; published July 5, 2013.

REFERENCES

Abramoff, M.D., Magalhaes, P.J., and Ram, S.J. (2004). Image processing with ImageJ. Biophotonics International **11:** 36–42.

Adams, P.D., et al. (2010). PHENIX: A comprehensive Python-based system for macromolecular structure solution. Acta Crystallogr. D Biol. Crystallogr. **66:** 213–221.

Alonso, A., Rojas, A., Godzik, A., and Mustelin, T. (2003). The Dual-Specific Protein Tyrosine Phosphatase Family. (Berlin: Springer).

Baunsgaard, L., Lütken, H., Mikkelsen, R., Glaring, M.A., Pham, T.T., and Blennow, A. (2005). A novel isoform of glucan, water dikinase phosphorylates pre-phosphorylated alpha-glucans and is involved in starch degradation in *Arabidopsis*. Plant J. **41:** 595–605.

Begley, M.J., Taylor, G.S., Brock, M.A., Ghosh, P., Woods, V.L., and Dixon, J.E. (2006). Molecular basis for substrate recognition by MTMR2, a myotubularin family phosphoinositide phosphatase. Proc. Natl. Acad. Sci. USA **103:** 927–932.

Blennow, A., Bay-Smidt, A.M., Olsen, C.E., and Møller, B.L. (2000). The distribution of covalently bound phosphate in the starch granule in relation to starch crystallinity. Int. J. Biol. Macromol. **27:** 211–218.

Blennow, A., and Engelsen, S.B. (2010). Helix-breaking news: Fighting crystalline starch energy deposits in the cell. Trends Plant Sci. **15:** 236–240.

Blennow, A., Mette Bay-Smidt, A., and Bauer, R. (2001). Amylopectin aggregation as a function of starch phosphate content studied by size exclusion chromatography and on-line refractive index and light scattering. Int. J. Biol. Macromol. **28:** 409–420.

Blennow, A., Nielsen, T.H., Baunsgaard, L., Mikkelsen, R., and Engelsen, S.B. (2002). Starch phosphorylation: A new front line in starch research. Trends Plant Sci. **7:** 445–450.

Boraston, A.B., Bolam, D.N., Gilbert, H.J., and Davies, G.J. (2004). Carbohydrate-binding modules: Fine-tuning polysaccharide recognition. Biochem. J. **382:** 769–781.

Bozonnet, S., Jensen, M.T., Nielsen, M.M., Aghajari, N., Jensen, M.H., Kramhøft, B., Willemoës, M., Tranier, S., Haser, R., and Svensson, B. (2007). The 'pair of sugar tongs' site on the non-catalytic domain C of barley alpha-amylase participates in substrate binding and activity. FEBS J. **274:** 5055–5067.

Buléon, A., Colonna, P., Planchot, V., and Ball, S. (1998). Starch granules: Structure and biosynthesis. Int. J. Biol. Macromol. **23:** 85–112.

Cantarel, B.L., Coutinho, P.M., Rancurel, C., Bernard, T., Lombard, V., and Henrissat, B. (2009). The Carbohydrate-Active EnZymes database (CAZy): An expert resource for glycogenomics. Nucleic Acids Res. **37** (Database issue)**:** D233–D238.

Caspar, T., Lin, T.P., Kakefuda, G., Benbow, L., Preiss, J., and Somerville, C. (1991). Mutants of *Arabidopsis* with altered regulation of starch degradation. Plant Physiol. **95:** 1181–1188.

Comparot-Moss, S., et al. (2010). A putative phosphatase, LSF1, is required for normal starch turnover in *Arabidopsis* leaves. Plant Physiol. **152:** 685–697.

Coutinho, P.M., and Henrissat, B. (1999). Carbohydrate-active enzymes: An integrated database approach. Recent Advances in Carbohydrate Bioengineering, **246:** 3–12.

Cuyvers, S., Dornez, E., Delcour, J.A., and Courtin, C.M. (2012). Occurrence and functional significance of secondary carbohydrate binding sites in glycoside hydrolases. Crit. Rev. Biotechnol. **32:** 93–107.

Davis, I.W., Leaver-Fay, A., Chen, V.B., Block, J.N., Kapral, G.J., Wang, X., Murray, L.W., Arendall, W.B., III., Snoeyink, J., Richardson, J.S., and Richardson, D.C. (2007). MolProbity: all-atom contacts and structure validation for proteins and nucleic acids. Nucleic Acids Res. **35** (Web Server issue)**:** W375–W383.

Dukhande, V.V., Rogers, D.M., Romá-Mateo, C., Donderis, J., Marina, A., Taylor, A.O., Sanz, P., and Gentry, M.S. (2011). Laforin, a dual specificity phosphatase involved in Lafora disease, is present mainly as monomeric form with full phosphatase activity. PLoS ONE **6:** e24040.

Edner, C., Li, J., Albrecht, T., Mahlow, S., Hejazi, M., Hussain, H., Kaplan, F., Guy, C., Smith, S.M., Steup, M., and Ritte, G. (2007). Glucan, water dikinase activity stimulates breakdown of starch granules by plastidial beta-amylases. Plant Physiol. **145:** 17–28.

Emsley, P., Lohkamp, B., Scott, W.G., and Cowtan, K. (2010). Features and development of Coot. Acta Crystallogr. D Biol. Crystallogr. **66:** 486–501.

Fettke, J., Hejazi, M., Smirnova, J., Höchel, E., Stage, M., and Steup, M. (2009). Eukaryotic starch degradation: Integration of plastidial and cytosolic pathways. J. Exp. Bot. **60:** 2907–2922.

Gallant, D.J., Bouchet, B., and Baldwin, P.M. (1997). Microscopy of starch: Evidence of a new level of granule organization. Carbohydr. Polym. **32:** 177–191.

Ganesh, S., Tsurutani, N., Suzuki, T., Hoshii, Y., Ishihara, T., Delgado-Escueta, A.V., and Yamakawa, K. (2004). The carbohydrate-binding domain of Lafora disease protein targets Lafora polyglucosan bodies. Biochem. Biophys. Res. Commun. **313:** 1101–1109.

Gentry, M.S., Dixon, J.E., and Worby, C.A. (2009). Lafora disease: Insights into neurodegeneration from plant metabolism. Trends Biochem. Sci. **34:** 628–639.

Gentry, M.S., Dowen, R.H., III., Worby, C.A., Mattoo, S., Ecker, J.R., and Dixon, J.E. (2007). The phosphatase laforin crosses evolutionary boundaries and links carbohydrate metabolism to neuronal disease. J. Cell Biol. **178:** 477–488.

Gentry, M.S., and Pace, R.M. (2009). Conservation of the glucan phosphatase laforin is linked to rates of molecular evolution and the glucan metabolism of the organism. BMC Evol. Biol. **9:** 138.

Glaring, M.A., Baumann, M.J., Abou Hachem, M., Nakai, H., Nakai, N., Santelia, D., Sigurskjold, B.W., Zeeman, S.C., Blennow, A., and Svensson, B. (2011). Starch-binding domains in the CBM45 family—Low-affinity domains from glucan, water dikinase and α-amylase involved in plastidial starch metabolism. FEBS J. **278:** 1175–1185.

Hansen, P.I., Spraul, M., Dvortsak, P., Larsen, F.H., Blennow, A., Motawia, M.S., and Engelsen, S.B. (2009). Starch phosphorylation—Maltosidic restrains upon 3′- and 6′-phosphorylation investigated by chemical synthesis, molecular dynamics and NMR spectroscopy. Biopolymers **91:** 179–193.

Hasegawa, H., and Holm, L. (2009). Advances and pitfalls of protein structural alignment. Curr. Opin. Struct. Biol. **19:** 341–348.

Hejazi, M., Fettke, J., Kötting, O., Zeeman, S.C., and Steup, M. (2010). The Laforin-like dual-specificity phosphatase SEX4 from *Arabidopsis* hydrolyzes both C6- and C3-phosphate esters introduced by starch-related dikinases and thereby affects phase transition of alpha-glucans. Plant Physiol. **152:** 711–722.

Holm, L., and Rosenström, P. (2010). Dali server: conservation mapping in 3D. Nucleic Acids Res. **38** (Web Server issue)**:** W545–W549.

Jia, Z., Barford, D., Flint, A.J., and Tonks, N.K. (1995). Structural basis for phosphotyrosine peptide recognition by protein tyrosine phosphatase 1B. Science **268:** 1754–1758.

Jung, S.K., Jeong, D.G., Yoon, T.S., Kim, J.H., Ryu, S.E., and Kim, S.J. (2007). Crystal structure of human slingshot phosphatase 2. Proteins **68:** 408–412.

Kadziola, A., Søgaard, M., Svensson, B., and Haser, R. (1998). Molecular structure of a barley alpha-amylase-inhibitor complex: Implications for starch binding and catalysis. J. Mol. Biol. **278:** 205–217.

Keeling, P.L., and Myers, A.M. (2010). Biochemistry and genetics of starch synthesis. Annu. Rev. Food Sci. Technol. **1:** 271–303.

Kerk, D., Conley, T.R., Rodriguez, F.A., Tran, H.T., Nimick, M., Muench, D.G., and Moorhead, G.B. (2006). A chloroplast-localized dual-specificity protein phosphatase in *Arabidopsis* contains a phylogenetically dispersed and ancient carbohydrate-binding domain, which binds the polysaccharide starch. Plant J. **46:** 400–413.

Koropatkin, N.M., and Smith, T.J. (2010). SusG: A unique cell-membrane-associated alpha-amylase from a prominent human gut symbiont targets complex starch molecules. Structure **18:** 200–215.

Kötting, O., Kossmann, J., Zeeman, S.C., and Lloyd, J.R. (2010). Regulation of starch metabolism: The age of enlightenment? Curr. Opin. Plant Biol. **13:** 321–329.

Kötting, O., Pusch, K., Tiessen, A., Geigenberger, P., Steup, M., and Ritte, G. (2005). Identification of a novel enzyme required for starch metabolism in *Arabidopsis* leaves. The phosphoglucan, water dikinase. Plant Physiol. **137:** 242–252.

Kötting, O., Santelia, D., Edner, C., Eicke, S., Marthaler, T., Gentry, M.S., Comparot-Moss, S., Chen, J., Smith, A.M., Steup, M., Ritte, G., and Zeeman, S.C. (2009). STARCH-EXCESS4 is a laforin-like Phosphoglucan phosphatase required for starch degradation in *Arabidopsis thaliana*. Plant Cell **21:** 334–346.

Lee, B., and Richards, F.M. (1971). The interpretation of protein structures: Estimation of static accessibility. J. Mol. Biol. **55:** 379–400.

Machovic, M., and Janecek, S. (2006). Starch-binding domains in the post-genome era. Cell. Mol. Life Sci. **63:** 2710–2724.

Minassian, B.A., et al. (1998). Mutations in a gene encoding a novel protein tyrosine phosphatase cause progressive myoclonus epilepsy. Nat. Genet. **20:** 171–174.

Moorhead, G.B., De Wever, V., Templeton, G., and Kerk, D. (2009). Evolution of protein phosphatases in plants and animals. Biochem. J. **417:** 401–409.

Muhrbeck, P., and Eliasson, A. (1991). Influence on the naturally occuring phosphate esters on the crystallinity of potato starch. J. Sci. Food Agric. **55:** 13–18.

Murshudov, G.N., Vagin, A.A., and Dodson, E.J. (1997). Refinement of macromolecular structures by the maximum-likelihood method. Acta Crystallogr. D Biol. Crystallogr. **53:** 240–255.

Nielsen, M.M., Bozonnet, S., Seo, E.S., Mótyán, J.A., Andersen, J.M., Dilokpimol, A., Abou Hachem, M., Gyémánt, G., Naested, H., Kandra, L., Sigurskjold, B.W., and Svensson, B. (2009). Two secondary carbohydrate binding sites on the surface of barley alpha-amylase 1 have distinct functions and display synergy in hydrolysis of starch granules. Biochemistry **48:** 7686–7697.

Niittylä, T., Comparot-Moss, S., Lue, W.L., Messerli, G., Trevisan, M., Seymour, M.D., Gatehouse, J.A., Villadsen, D., Smith, S.M., Chen, J., Zeeman, S.C., and Smith, A.M. (2006). Similar protein phosphatases control starch metabolism in plants and glycogen metabolism in mammals. J. Biol. Chem. **281:** 11815–11818.

Otwinowski, Z., and Minor, W. (1997). Processing of X-ray diffraction data collected in oscillation mode. Method. Enzymol. **276:** 307–326.

Payan, F., and Qian, M. (2003). Crystal structure of the pig pancreatic alpha-amylase complexed with malto-oligosaccharides. J. Protein Chem. **22:** 275–284.

Ragunath, C., Manuel, S.G., Venkataraman, V., Sait, H.B., Kasinathan, C., and Ramasubbu, N. (2008). Probing the role of aromatic residues at the secondary saccharide-binding sites of human salivary alpha-amylase in substrate hydrolysis and bacterial binding. J. Mol. Biol. **384:** 1232–1248.

Ritte, G., Heydenreich, M., Mahlow, S., Haebel, S., Kötting, O., and Steup, M. (2006). Phosphorylation of C6- and C3-positions of glucosyl residues in starch is catalysed by distinct dikinases. FEBS Lett. **580:** 4872–4876.

Ritte, G., Lloyd, J.R., Eckermann, N., Rottmann, A., Kossmann, J., and Steup, M. (2002). The starch-related R1 protein is an alpha-glucan, water dikinase. Proc. Natl. Acad. Sci. USA **99:** 7166–7171.

Roach, P.J. (2002). Glycogen and its metabolism. Curr. Mol. Med. **2:** 101–120.

Robert, X., Haser, R., Mori, H., Svensson, B., and Aghajari, N. (2005). Oligosaccharide binding to barley alpha-amylase 1. J. Biol. Chem. **280:** 32968–32978.

Santelia, D., Kötting, O., Seung, D., Schubert, M., Thalmann, M., Bischof, S., Meekins, D.A., Lutz, A., Patron, N., Gentry, M.S., Allain, F.H., and Zeeman, S.C. (2011). The phosphoglucan phosphatase like sex Four2 dephosphorylates starch at the C3-position in *Arabidopsis*. Plant Cell **23:** 4096–4111.

Santelia, D., and Zeeman, S.C. (2011). Progress in *Arabidopsis* starch research and potential biotechnological applications. Curr. Opin. Biotechnol. **22:** 271–280.

Schrodinger, LLC. (2010). The PyMOL Molecular Graphics System, Version 1.3.

Serratosa, J.M., et al. (1999). A novel protein tyrosine phosphatase gene is mutated in progressive myoclonus epilepsy of the Lafora type (EPM2). Hum. Mol. Genet. **8:** 345–352.

Sevcík, J., Hostinová, E., Solovicová, A., Gasperík, J., Dauter, Z., and Wilson, K.S. (2006). Structure of the complex of a yeast glucoamylase with acarbose reveals the presence of a raw starch binding site on the catalytic domain. FEBS J. **273:** 2161–2171.

Sherwood, A.R., Paasch, B.C., Worby, C.A., and Gentry, M.S. (2013). A malachite green-based assay to assess glucan phosphatase activity. Anal. Biochem. **435:** 54–56.

Sokolov, L.N., Dominguez-Solis, J.R., Allary, A.L., Buchanan, B.B., and Luan, S. (2006). A redox-regulated chloroplast protein phosphatase binds to starch diurnally and functions in its accumulation. Proc. Natl. Acad. Sci. USA **103:** 9732–9737.

Streb, S., and Zeeman, S.C. (2012). Starch metabolism in *Arabidopsis*. In The Arabidopsis Book **10:** e0160, doi/10.1199/tab.0160.

Tagliabracci, V.S., Turnbull, J., Wang, W., Girard, J.M., Zhao, X., Skurat, A.V., Delgado-Escueta, A.V., Minassian, B.A., Depaoli-Roach, A.A., and Roach, P.J. (2007). Laforin is a glycogen phosphatase, deficiency of which leads to elevated phosphorylation of glycogen in vivo. Proc. Natl. Acad. Sci. USA **104:** 19262–19266.

Takeda, Y, and Hizukuri, S. (1981). Studies on starch phosphate. Part 5. Reexamination of the action of sweet-potato bet-amylase on phosphorylated (1->4)-a-D-glucan. Carbohydr. Res. **89:** 174–178.

Tester, R.F., Karkalas, J., and Qi, X. (2004). Starch - Composition, fine structure and architechture. J. Cereal Sci. **39:** 151–165.

Tonks, N.K. (2006). Protein tyrosine phosphatases: From genes, to function, to disease. Nat. Rev. Mol. Cell Biol. **7:** 833–846.

Tonks, N.K. (2013). Special issue: Protein phosphatases: From molecules to networks: Introduction. FEBS J. **280:** 323.

Vander Kooi, C.W., Taylor, A.O., Pace, R.M., Meekins, D.A., Guo, H.F., Kim, Y., and Gentry, M.S. (2010). Structural basis for the glucan phosphatase activity of Starch Excess4. Proc. Natl. Acad. Sci. USA **107:** 15379–15384.

Wang, W., and Roach, P.J. (2004). Glycogen and related polysaccharides inhibit the laforin dual-specificity protein phosphatase. Biochem. Biophys. Res. Commun. **325:** 726–730.

Winn, M.D., et al. (2011). Overview of the CCP4 suite and current developments. Acta Crystallogr. D Biol. Crystallogr. **67:** 235–242.

Worby, C.A., Gentry, M.S., and Dixon, J.E. (2006). Laforin, a dual specificity phosphatase that dephosphorylates complex carbohydrates. J. Biol. Chem. **281:** 30412–30418.

Xiao, J., Engel, J.L., Zhang, J., Chen, M.J., Manning, G., and Dixon, J.E. (2011). Structural and functional analysis of PTPMT1, a phosphatase required for cardiolipin synthesis. Proc. Natl. Acad. Sci. USA **108:** 11860–11865.

Yu, T.S., et al. (2001). The *Arabidopsis* sex1 mutant is defective in the R1 protein, a general regulator of starch degradation in plants, and not in the chloroplast hexose transporter. Plant Cell **13:** 1907–1918.

Yuvaniyama, J., Denu, J.M., Dixon, J.E., and Saper, M.A. (1996). Crystal structure of the dual specificity protein phosphatase VHR. Science **272:** 1328–1331.

Zeeman, S.C., Tiessen, A., Pilling, E., Kato, K.L., Donald, A.M., and Smith, A.M. (2002). Starch synthesis in *Arabidopsis*. Granule synthesis, composition, and structure. Plant Physiol. **129:** 516–529.

Zhou, G., Denu, J.M., Wu, L., and Dixon, J.E. (1994). The catalytic role of Cys124 in the dual specificity phosphatase VHR. J. Biol. Chem. **269:** 28084–28090.